19-10-2012

Mechanism of secondary currents in open channel flows

Shu-Qing Yang
University of Wollongong, shuqing@uow.edu.au

Soon Keat Tan
Nanyang Technological University, Singapore

Xi-Kun Wang
Nanyang Technological University, Singapore

Mechanism of secondary currents in open channel flows

Abstract

This paper describes the conditions for initiation and maintenance of secondary currents in open channel flows. By analyzing the Reynolds equation in the wall-normal and wall-tangent directions, this study reveals that, like other types of vortices, the secondary currents are originated in the near-boundary region, and the magnitude (or strength) of secondary flow is proportional to the lateral gradient of near-wall velocity. The near-wall secondary flow always moves from the region with lower velocity (or lower boundary shear stress) to the location with higher velocity (or higher boundary shear stress). Subsequently, the near-boundary secondary flow creeps into the main flow and drives circulation within a region enclosed by lines of zero total shear stress, leading to anisotropy of turbulence in the main flow region. This paper also discusses typical secondary currents in open channel flows and presents the relationship between sediment transport and secondary currents. The formation of sand ridges widely observed on the Earth surface is explained in the light of the proposed relationship.

Keywords

mechanism, secondary, flows, currents, open, channel

Disciplines

Medicine and Health Sciences | Social and Behavioral Sciences

Publication Details

Yang, S., Tan, S. Keat. & Wang, X. (2012). Mechanism of secondary currents in open channel flows. Journal of Geophysical Research, 117 (F4), 1-13.

Mechanism of secondary currents in open channel flows

Shu-Qing Yang,[1] Soon Keat Tan,[2] and Xi-Kun Wang[3]

Received 4 June 2012; revised 31 August 2012; accepted 5 September 2012; published 19 October 2012.

[1] This paper describes the conditions for initiation and maintenance of secondary currents in open channel flows. By analyzing the Reynolds equation in the wall-normal and wall-tangent directions, this study reveals that, like other types of vortices, the secondary currents are originated in the near-boundary region, and the magnitude (or strength) of secondary flow is proportional to the lateral gradient of near-wall velocity. The near-wall secondary flow always moves from the region with lower velocity (or lower boundary shear stress) to the location with higher velocity (or higher boundary shear stress). Subsequently, the near-boundary secondary flow creeps into the main flow and drives circulation within a region enclosed by lines of zero total shear stress, leading to anisotropy of turbulence in the main flow region. This paper also discusses typical secondary currents in open channel flows and presents the relationship between sediment transport and secondary currents. The formation of sand ridges widely observed on the Earth surface is explained in the light of the proposed relationship.

Citation: Yang, S.-Q., S. K. Tan, and X.-K. Wang (2012), Mechanism of secondary currents in open channel flows, *J. Geophys. Res.*, *117*, F04014, doi:10.1029/2012JF002510.

1. Introduction

[2] River channels, deserts and continental shelves often possess sand ridges, i.e., the longitudinal bed forms that are aligned parallel to the direction of mean flow [*Karcz*, 1981]. These longitudinal bed forms take the form of periodic, lateral variations in bed texture (termed sediment strips) and bed topography (termed sand ridges). These phenomena have been widely observed in nature, for example in gravel bed rivers [*Tsujimoto*, 1989; *Sambrook Smith and Ferguson*, 1996], ephemeral streambeds [*Culbertson*, 1967], estuaries [*Williams et al.*, 2008; *Carling et al.*, 2009], continental shelves [*Kenyon*, 1970; *Karl*, 1980] and deserts [*Liao et al.*, 2010]. These researchers observed that the existence of ridges is always associated with secondary currents [*Colombini*, 1993; *Nezu et al.*, 1988]. Therefore, to understand how the sand ridges are formed, one must first understand the mechanism of secondary currents.

[3] *Prandtl* [1952] identified that there are two categories of steady secondary currents in fluid flow. Secondary currents of the first kind or skew-induced streamwise vorticity, originated from the mean flow but driven by the curvature effect [e.g., *Blanckaert and Graf*, 2004], are well understood. Secondary currents of the second kind, as observed in straight and non-circular channels, are generated by turbulence that is related to the formation of sand ridges [e.g., *Colombini*, 1993]. In this paper, we deal with secondary currents of the second kind. During Prandtl's time, only secondary currents of the second kind induced by corners were identified. Such corner-induced secondary currents have been characterized by flow moving into the apex of the corner with a return flow moving away from the corner and along the channel boundaries. This concept is also termed as the 'corner'-induced secondary currents [*Perkins*, 1970; *Gessner* 1973; *Galletti and Bottaro*, 2004]. The corner vortices are damped rapidly within a short distance from the sidewalls. *Nezu and Rodi* [1985] experimentally showed that a channel may remain free from secondary currents beyond the sidewall region.

[4] In 1980s, several researchers found that secondary currents can also be generated without "corners," if the channel bed is slightly perturbed. *Nezu and Rodi* [1985] experimental results showed that lateral (or spanwise) variations in bed topography and roughness can lead to the formation of secondary currents, which are independent of the sidewall effect or the corner induced secondary currents [*Nezu and Nakagawa*, 1993; *Wang and Cheng*, 2005]. Up to now, the mechanism of the secondary currents (either corner- or bed-induced) is still being debated.

[5] The vorticity equation governing the secondary currents has the following form:

$$V\frac{\partial \Omega}{\partial y}+W\frac{\partial \Omega}{\partial z}=\frac{\partial^2}{\partial y\partial z}\left(\overline{v'^2}-\overline{w'^2}\right)+\left(\frac{\partial^2}{\partial z^2}-\frac{\partial^2}{\partial y^2}\right)\overline{vw}+\nu\nabla^2\Omega \tag{1a}$$

$$\Omega=\frac{\partial W}{\partial y}-\frac{\partial V}{\partial z} \tag{1b}$$

[1]School of Civil, Mining and Environmental Engineering, University of Wollongong, Wollongong, New South Wales, Australia.
[2]Nanyang Environment and Water Research Institute, Nanyang Technological University, Singapore.
[3]Maritime Research Center, School of Civil and Environmental Engineering, Nanyang Technological University, Singapore.

Corresponding author: S.-Q. Yang, School of Civil, Mining and Environmental Engineering, University of Wollongong, Wollongong, NSW 2522, Australia. (shuqing@uow.edu.au)

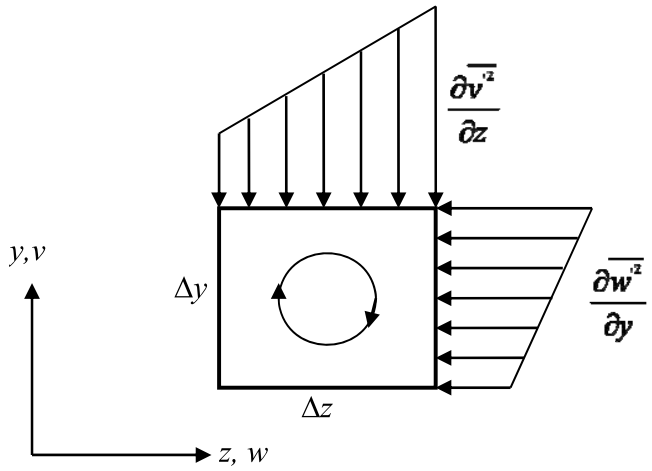

Figure 1. Vorticity production by the imbalance of normal stress, after *Perkins* [1970]. This is used to support Einstein's postulation that formation of secondary currents is caused by anisotropic turbulent velocity, and has no direct relationship with the mean flow and boundary.

where Ω is the vorticity, V and W are the mean velocities of secondary currents in vertical (y) and spanwise (z) directions, respectively. v and w are the velocity fluctuations and ν is the kinematic viscosity. Based on equations (1a) and (1b), *Einstein and Li* [1956] ascribed the origin of corner-related secondary currents in straight channel flows to the first term on the Right-hand-side (RHS) of equation (1a), i.e., the imbalance of the normal Reynolds stresses in a cross-sectional plane perpendicular to the streamwise direction, because they realized that the second and third terms of RHS are negligible. This exposition was followed by *Brundrett and Baines* [1964] and others (see *Gerard* [1978] and *Bradshaw* [1987] for an extensive review). *Perkins* [1970] used Figure 1 to explain Einstein and Li's postulation about the formation of secondary currents, i.e.,

[6] (a) the imbalance of normal Reynolds stress in the main flow region generates the secondary currents, whereas the boundary does not play any main role, and (b) the driving force of secondary currents is the variation of turbulent velocity, not the mean velocity.

[7] The mechanism of secondary currents proposed by *Einstein and Li* [1956] is not universal and has been found invalid by many researchers including *Gessner* [1973], *Tamburrino and Gulliver* [1999], *Bradshaw* [1987] and *Gavrilakis* [1992]. *Nezu and Nakagawa* [1993] also remarked that "*the mechanisms for initiation and maintenance of cellular secondary currents in wide channel flows are not yet well understood.*"

[8] The role of the boundary in the formation of secondary current has been hotly debated. *Rodriguez and Garcia* [2008] observed the multicellular structures in a very wide channel with smooth sidewalls and a rough bed. The formation of these multicellular structures was attributed to the large gradient in roughness between a smooth glass wall and the gravel bed. This is consistent with the result of *Cooper and Tait* [2008] who showed that high-speed longitudinal streaks exist over water-worked gravel beds. They perceived that the origin of secondary currents is the result of variation of bed roughness or topography. *Albayrak*'s [2008] study also implied that the secondary currents may hinge on the bed roughness. However, none of these studies has provided a theoretical explanation, and there are no published equations available in the literature to describe these observations.

[9] The above brief literature review clearly demonstrates that there are still knowledge gaps on the formation of secondary currents [*Nikora and Roy*, 2010]. The experimental observations reveal that the secondary currents are induced by lateral difference in roughness, while Einstein and other researchers ascribe the formation of secondary currents to the imbalance of normal stress. The main objectives of this study are to: (1) investigate the driving force of the secondary currents; (2) illustrate mathematically whether the boundary plays a crucial role in the formation of secondary currents; and (3) demonstrate the interactions of secondary currents, sediment transport and morpho-dynamics.

2. Theoretical Considerations

[10] For a steady and uniform flow, the continuity equation is

$$\frac{\partial V}{\partial y} + \frac{\partial W}{\partial z} = 0, \tag{2a}$$

and the momentum equation in the x-direction may be written as follows [*Yang*, 2007]

$$\frac{\partial(\rho UV - \tau_{xy})}{\partial y} + \frac{\partial(\rho UW - \tau_{xz})}{\partial z} = \rho g S \tag{2b}$$

where U is the time-average velocity in the x direction (see Figure 2), S is the energy slope, g is the gravitational acceleration. $\tau_{xy} = \mu \partial U/\partial y - \rho\overline{uv}$ and $\tau_{xz} = \mu \partial U/\partial z - \rho\overline{uw}$ in which μ = dynamic viscosity, ρ = fluid density, the over-bar denotes time-averaged values, u, v and w are the three components of the turbulent velocity fluctuations.

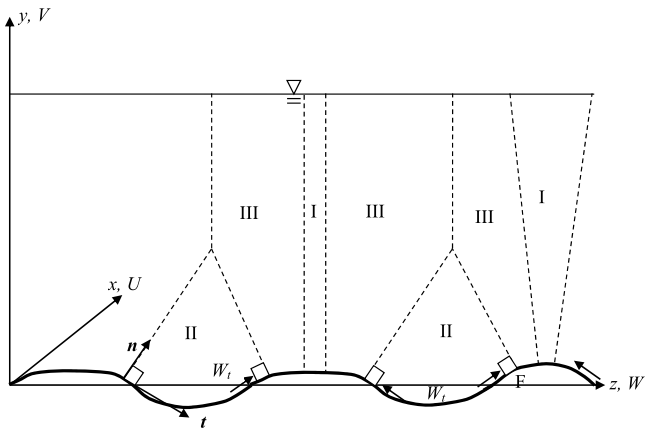

Figure 2. A flow domain can be divided into sub-regions depending on the boundary conditions. In sub-region I the boundary normal lines are not intersected; the normal lines in sub-region II are always intersected; and sub-region III locates between I and II, in which n is the unit vector of boundary normal line, t is the unit direction along the boundary tangential direction. W_t is the near-bed secondary flow and it is always in the boundary tangent direction.

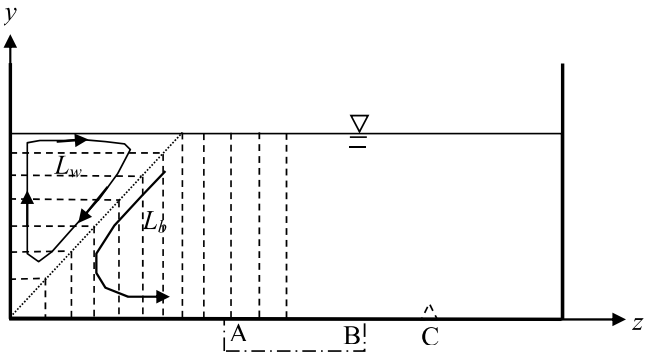

Figure 3. Schematic diagram of rectangular open channel flow, which can be considered as a special case of sub-region II in Figure 2. The turbulent characteristics at a certain point depends on the "nearest boundary," i.e., above the dotted line where the flow is dominated by the sidewall, and for the region below the dotted line where the bed plays a significant role for its flow characteristics; for a flow region between two dashed normal lines where the turbulent characteristics is mainly related with the wetted perimeter enclosed by the two normal lines. If the bed AB is lowered, then it becomes a compound channel. The triangle on point C is the imaginary roughness. L_b and L_w are the normal distance to the dotted division line from the bed and sidewall. Secondary currents are represented by solid lines with arrows.

[11] To estimate the influence of boundary on a uniform flow with an arbitrary bed as shown in Figure 2, the above equations may be rewritten as follows:

$$\frac{\partial V_n}{\partial n} + \frac{\partial W_t}{\partial t} = 0 \tag{3}$$

$$\frac{\partial(\rho U V_n - \tau_{xn})}{\partial n} + \frac{\partial(\rho U W_t - \tau_{xt})}{\partial t} = \rho g S \tag{4}$$

where n and t denote the wall-normal and wall-tangent directions. Likewise, the flow region shown in Figure 2 can be divided into many strip segments normal to the boundary. The convex, concave and the remaining segments are marked with "I," "II" and "III," respectively.

[12] Both equations (3) and (4) are valid in each strip. Noticing that the gradient in the wall-tangent direction is much less than that in the wall-normal direction, equation (4) may be simplified as follows:

$$\frac{\partial(\rho U V_n - \tau_{xn})}{\partial n} = \rho g S \tag{5}$$

$$\frac{\partial(\rho U W_t - \tau_{xt})}{\partial t} \approx 0. \tag{6}$$

In the main flow region, the simplification shown in equations (5) and (6) includes removal of the interactions between normal and tangential gradients in equation (4). Detailed investigation by *Yang and McCorquadale* [2004] indicated that this simplification can yield reasonable results and the incurred errors are negligible. Equations (5) and (6) convert the partial differential equations into ordinary differential equations for each sub-region enclosed by the boundary normal lines. In order to integrate equation (5) along a strip, one needs to determine its upper limit. The upper limit for sub-region I is the free surface. For sub-region II, every point in the field is formed by the intersection of two boundary normal lines. The surplus energy (=rate of energy supplied – rate of energy dissipated) from any volume of flow will be transported along a particular direction to the boundary and to be dissipated in order to maintain the energy balance of the system. Further, Yang and his coworkers [*Yang and McCorquadale*, 2004; *Lim and Yang*, 2005; *Yang and Lim*, 2005; *Yang et al.*, 2005a] postulated that this particular direction is along the normal line of boundary, i.e., the surplus energy will be transferred to the nearest boundary (shortest distance). They defined the dimensionless shortest distance as the ratio of geometrical normal distance (L) to the roughness height (d_{50}) or thickness of viscous sublayer (v/u_*). Figure 3 illustrates how to determine the upper limit of equation (5), in which the flow region is divided into many segments (dashed lines), and the dotted line in the corner can be obtained by equating the dimensionless distances to the sidewall and bed [*Yang and Lim*, 1997; *Yang and McCorquadale*, 2004]:

$$\frac{L_b}{v/u_{*_b}} = \frac{L_w}{v/u_{*_w}} \tag{7}$$

where L = geometrical distance from the dotted line (or division line) to the boundary; v = kinematic viscosity; u_* = shear velocity and the subscripts b and w refer to the bed and wall, respectively. Above the division line, the turbulent energy will be dissipated on the wall, and below it on the bed by friction. The slope of the division line $k = L_w/L_b$ can be determined by the equation proposed in *Yang and Lim* [1997]:

$$k^3 + (h/b)k - 2 = 0 \tag{8}$$

where h = water depth, and b = channel width. For a very wide channel, $h/b \approx 0$, and k approaches $\sqrt[3]{2} = 1.26$. This means that a pair of secondary currents exists on both sides of $z = 1.26y$, as illustrated clearly in *Tracy*'s [1965] experiment which is described briefly herein.

[13] *Tracy* [1965] measured the secondary currents in a channel with $h/b = 0.156$. His results confirm that a pair of secondary cells exists in the corner, at either side of a straight line $z = 1.2y$. Furthermore, *Tracy* [1965] showed that if $z > 1.2h$, the Reynolds shear stress is independent of z and follows the standard linear line

$$-\frac{\overline{uv}}{u_*^2} = 1 - \frac{y}{h}. \tag{9}$$

If $z < 1.2h$, the Reynolds shear stress no longer follows equation (9), and detailed discussion of the Reynolds shear stress will be presented in the following sections.

[14] For a very wide channel, *Knight and Patel* [1985] and *Rhodes and Knight* [1994] found that the measured mean

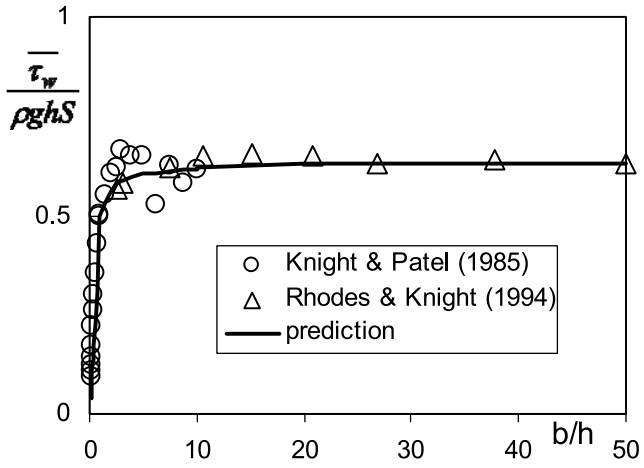

Figure 4. The measured (symbols) and calculated (the solid line) mean sidewall shear stresses [after *Yang and Lim*, 1997]. The normalized shear stress approaches to half of 1.26, implying that the division line in Figure 3 can be expressed by z = 1.26y.

sidewall shear stress (i.e., $\overline{\tau}_w/\rho ghS$) is constant and equal to 0.63 (see Figure 4). The mean sidewall shear stress is defined by

$$\bar{\tau}_w = \rho g S \frac{A_w}{p_w} \tag{10}$$

where p is the wetted perimeter, A is the area of water, and subscript w denotes the sidewall. As $p_w = h$, then A_w can be determined from equation (6) as follows

$$A_w = 0.63h^2 = \frac{1}{2}(1.26h)h \tag{11}$$

as the area of a triangle that is half of the base multiplied by the height. This special value of 1.26, which has been observed by other researchers as well (for example *Tracy* [1965]), elucidates that the spread of corner-related secondary current cell is within $z < 1.26h$ (also see Figure 5a). Equation (8) indicates that $k = 1$ or $z = y$ only when $b = 2h$. In that case the friction on sidewall is identical to that on the bed. In other words, the physical interpretation of 1.26 for the line at $z = 1.26y$ which subdivides the upper and lower corner cells is a consequence of different frictions on the bed and sidewall. It follows then the line $z = 1.26y$, similar to the free surface, is a soft boundary for secondary circulation. In the literature, other division lines have been proposed [see, e.g., *Flintham and Carling*, 1988, 1989].

3. Secondary Currents in Near-Boundary Region

[15] In this study, the momentum equation in the direction tangent to the boundary surface (either sidewall or bed) will be examined. In the near-boundary region, equation (6) must be satisfied strictly to meet its boundary conditions. By integrating equation (6) with respect to z, one obtains

$$UW_t - \nu\frac{\partial U}{\partial t} + \overline{uw_t} = 0. \tag{12}$$

In a laminar flow where $-\overline{uw_t} = 0$, equation (12) reads

$$W_t = (\nu \partial U/\partial z)/U. \tag{13}$$

Equation (13) shows that a velocity W_t may be generated once $\partial U/\partial z \neq 0$. In other words, a lateral velocity gradient in the near-bed region drives secondary currents in a laminar flow. It follows that turbulence anisotropy may not be a necessary condition for the generation of secondary currents. In fact, equation (13) clearly indicates that W_t will be generated as long as $\partial U/\partial z \neq 0$, and secondary currents ensued. It should also be stressed that, in the boundary region, this condition for cross-stream velocity generation is

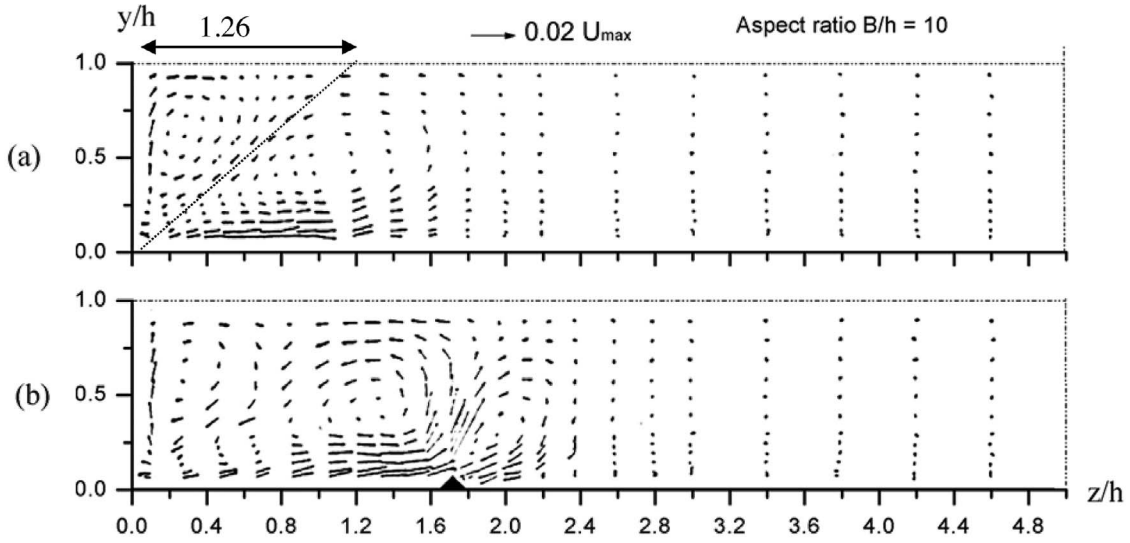

Figure 5. Distributions of the velocity vectors for cellular secondary currents induced by: (a) sidewall where the dotted line is z = 1.26y indicating that the flow is really dividable and the width of corner secondary cell spreads within 1.26 h; (b) longitudinal ridge [after *Nezu and Nakagawa*, 1993].

always valid as equation (12) must be satisfied. In the main flow, equations (5) and (6) are the approximate forms of equation (4) based on the assumption that the interaction of normal and tangential gradients is negligible.

[16] For a turbulent flow, the viscous effect is negligible. In the boundary region, equation (12) can be simplified as follows:

$$-UW_t - \overline{uw_t} = 0. \tag{14}$$

By drawing an analogy with the coefficient of molecular viscosity in Stokes's law, *Boussinesq* [1877] correlated the Reynolds shear stress and strain rate as follows:

$$-\overline{uw_t} = \varepsilon_t \frac{\partial U}{\partial t} \tag{15}$$

where ε_t is the transverse turbulent eddy viscosity. Equation (15) demonstrates that the Reynolds shear stress $-\overline{uw_t}$ is nonzero if $\partial U/\partial t \neq 0$. Inserting equation (15) in equation (14) gives

$$W_t = \frac{\varepsilon_t}{U} \frac{\partial U}{\partial t}. \tag{16}$$

Equation (16) states that the lateral component of secondary currents W_t is driven by the streamwise mean velocity gradient, i.e., $\partial U/\partial t$. The largest W_t –value always exists in the boundary region where U is minimum (i.e., $1/U$ in equation (16) is highest) and $\partial U/\partial t$ maximum. This fact implies that secondary currents originate from the boundary region as U in the boundary region is smaller than that in the main flow.

[17] In the viscous sublayer, the near-bed velocity U is proportional to the shear velocity $u^2_{*(z)}$ $(=\tau/\rho)$ and the velocity profile can be approximated using $U/u_* = u_* y/\nu$. From equation (16), non-uniform distribution of boundary shear stress $[\partial\tau/\partial z \neq 0]$ leads to nonzero W_t, or

$$W_t = \frac{\varepsilon_t}{\tau_{(z)}} \frac{d\tau_{(z)}}{dz} = \varepsilon_t \frac{d\ln\tau_{(z)}}{dz}. \tag{17}$$

Therefore, one may conclude that if a lateral variation of near-wall velocity/boundary shear stress exists, secondary flows will be induced and non-uniform distribution of boundary shear stress may be observed, as reported *by Knight and Patel* [1985] and *Rhodes and Knight* [1994].

[18] Equations (16) and (17) indicate that positive W_t will be formed if U or τ increases with t or in z-direction, and vice versa. In other words, the direction of near-bed secondary flow always moves from a location with low velocity to one with higher velocity. This is why corner-related secondary flow always moves outward along the channel boundaries (see Figure 3) away from the apex (velocity at apex $U = 0$). Alternatively as shown in Figure 2, the near-bed secondary flow always points to the location with higher boundary shear stress: the boundary shear stress of sub-region I is higher than that in sub-region II, and hence W_t drives sediment particles upward to the crest. In this way, sand ridges are formed by the secondary flow.

[19] For a homogenous channel boundary (e.g., Figure 3), the velocity gradient $\partial U/\partial z$ in the region $z > 1.26h$ is much smaller compared to that at the corner. This is why the measured secondary currents in the central region are much weaker, as observed by *Nezu and Nakagawa* [1993] and their measurement results are reproduced in Figure 5a. These authors also found that secondary currents are discernible at the same region where nonzero $\partial U/\partial z$ is induced by some disturbances on the bed (artificial ridges) or non-uniform roughness (see Figure 5b).

[20] Equation (17) shows that the near-wall secondary flow always moves toward the location where the shear stress is higher (i.e., $\partial\tau/\partial z > 0$). Equation (17) also indicates that secondary flow will not be observed if the boundary shear stress is uniform in the spanwise direction. The converse is also true.

[21] The maximum or minimum boundary shear stress occurs at the location where $d\tau/dz = 0$ and $W_t = 0$. This location may be determined by differentiating equation (17) with respect to z, and setting it to zero, i.e.,

$$\varepsilon_t \frac{d^2\tau}{dz^2} = \tau \frac{dW_t}{dz} + W_t \frac{d\tau}{dz}. \tag{18}$$

It can be further deduced from equation (18) that $d^2\tau/dz^2$ is positive when the secondary flow is upward (or $dW_t/dz > 0$), and negative when it is downward.

[22] *Webel and Schatzmann* [1984] measured the lateral eddy viscosity ε_t in an open channel, and found that $\varepsilon_t/(u_* h)$ is constant and is equal to 0.177. Thus equation (17) can be rewritten as follows:

$$\frac{W_t}{u_*} = \frac{\varepsilon_t}{u_* h} \frac{h}{\tau} \frac{d\tau}{dz} = 0.177 \frac{h}{\tau_b} \frac{d\tau_b}{dz}. \tag{19}$$

Yang and Lim [1997, 1998] showed that the boundary shear stress along a corner can be simplified as a linear distribution, i.e., $d\tau/dz \approx \rho g S$ and $\tau_b < \rho g h S$, where ρ = density of fluid, h = water depth in Figure 3. Thus equation (19) may be simplified as

$$\frac{W_t}{u_*} \approx 0.177. \tag{20}$$

For most experimental flows, $U/u_* = 15\sim20$, where U is the cross-sectional average velocity. Assuming an average value of $U/u_* \approx 17.7$, then one may deduce from equation (20) that the magnitude of secondary flow is

$$\frac{W_t}{U} \approx 1\% \tag{21}$$

and this magnitude is consistent with the reported value in the literature [e.g., *Nezu and Nakagawa*, 1993].

[23] Consider a very wide channel as shown in Figure 3. If the channel boundary is homogenous, no secondary circulation is observed in the central region. If the homogenous bed is replaced by a heterogeneous boundary, for example the boundary is changed slightly by lowering/rising "AB" or roughness at "C" is incorporated on the boundary, lateral gradient of near-bed velocity is created, i.e., $\partial U/\partial z \neq 0$ at these points. Then, according to equations (16) and (17), secondary currents will be generated. *Einstein and Li*'s [1956] theory does not indicate the existence of secondary currents especially when the roughness size is too small to affect the main flow turbulence. This situation has in fact been demonstrated conclusively by *Nezu and Nakagawa*'s

Table 1. Summary of Turbulent Structures of Cellular Secondary Currents in Open Channels[a]

Type	Upflow Region ($v > 0$)	Downflow Region ($v < 0$)
Primary mean velocity	Low	High
Bed shear stress	Low	High
Turbulence intensity farther from the bed	High	Low
Reynolds shear stress farther from the bed	High	Low
Suspended load	High	Low
Bed load	Low	High
On water surface	Boil lines, divergence	Foam lines, convergence
River bed form	Ridges	Troughs
Bed roughness	Fine sand, smooth bed strips	Coarse sand, rough bed strips

[a]After *Nezu and Nakagawa* [1993].

[1993] measurements in a channel with an aspect ratio of $b/h = 10$. The results are shown in Figure 5a: (1) no secondary currents is observed in the central part in the case of smooth boundary condition, and (2) when the boundary is slightly disturbed using a very small triangular longitudinal ridge, a secondary flow is formed immediately (see Figure 5b), as stipulated by equation (16) or (17). This is concrete evidence that larger and isolated bed roughness elements such as sand ridges may increase the strength of secondary flow. One may also deduce from equation (16) that the magnitude of secondary flow does not increase with the size of the roughness, but instead depends on the non-uniform distribution of the roughness elements. For instance, the secondary currents in Figure 5b may disappear if the roughness elements are uniformly distributed along the wetted perimeter.

4. Secondary Currents in the Main Flow Region

[24] For every stripe as shown in Figures 2 and 3, equations (5) and (6) are strictly satisfied in the near-boundary region, but they are only approximately true in the main flow region. It is necessary to discuss how the near-bed tangential velocity W_t evolves and generates secondary flow cells in the main flow region.

[25] By definition, fluid particles flow tangentially at the free surface, division lines and solid boundary. Thus the wall-tangent velocity W_t has to change its direction when it encounters these interfaces. The total shear stress must be zero along these lines [*Yang and Lim*, 2006], i.e.,

$$UV_n - \nu\frac{\partial U}{\partial n} + \overline{uv_n} = 0 \tag{22}$$

where n refers to the normal direction of division line. As a result, the secondary flow is confined within the region prescribed by these interfaces and a recirculation pattern is formed.

[26] As the tangential velocity W_t drives a circulation, the wall-normal velocity V_n will be induced in the main flow region, and its influence on the Reynolds shear stress may be estimated using equation (23) which is derived by integrating equation (5), i.e.

$$-\frac{\overline{uv}}{u_*^2} = \left(1 - \frac{y}{h}\right) + \frac{UV_n}{u_*^2}. \tag{23}$$

Equation (23) states that $-\overline{uv}/u_*^2$ varies with the secondary currents. While W_t plays an important role in the near-boundary region, V_n dominates, in the main flow region, the momentum and mass transfer. It can be further inferred that the Reynolds normal stresses u, v and w will evolve correspondingly. It follows that turbulence anisotropy may not be the necessary condition for the generation of secondary currents. This is analogous to pipe or boundary layer flows, in which the existence of turbulence is always associated with the solid wall. Without the wall, all eddies including the secondary currents will disappear and the flow can be treated as ideal or potential flows, and this is the basis of *Prandtl*'s [1905] boundary layer flows, which refers to a thin layer near the surface, where friction is dominant, and an inviscid flow external to the boundary layer, where friction is negligible. In other words, the boundary layer is responsible for all types of eddies due to friction, the "inviscid layer" where Euler's equation can be applied is free of eddies.

[27] Equation (23) indicates that in the main flow region, only V_n, and not W_t, is involved in momentum transfer that will affect mass and energy transfer. This deduction is consistent with *Nezu and Nakagawa*'s [1993] observations as shown in Table 1.

[28] If the boundary region is the source of the secondary currents, then the strength of secondary flow will be the maximum in the wall region, and will become smaller in the main flow region as it is induced by W_t. Likewise, if the main flow region is the source of secondary currents as shown in Figure 1, then the magnitude of secondary flow in the main flow region must be higher than that in the near-wall region. Therefore, one can infer the source of secondary currents by examining the strength of secondary currents. *Nezu and Nakagawa* [1993, p. 115] observed that "*the secondary currents are larger near the bed than near the free surface.*" From Figure 5, one can also conclude that the maximum strength of secondary currents always appears in the near-wall region, or more precisely the maximum strength of secondary flow always corresponds to the location where $\partial U/\partial z$ is the maximum.

[29] In Figure 3, if the boundary at "AB" is lowered, the rectangular channel becomes a compound channel, which is similar to natural rivers that have a main channel and floodplains. A number of experimental and numerical studies have been performed on compound channels, see a comprehensive review by *Shiono and Knight* [1991]. All research to date show that secondary currents are observed in compound channels, and the maximum strength is always observed at the interface between the main channel and the floodplains where $\partial U/\partial z$ = max. For a very wide floodplain where the water depth remains constant laterally, then $\partial U/\partial z \approx 0$, and equation (16) predicts that the secondary currents in this region (far away from the main channel) are too weak to be discernible. Referring to Figure 3 and in the main channel, at

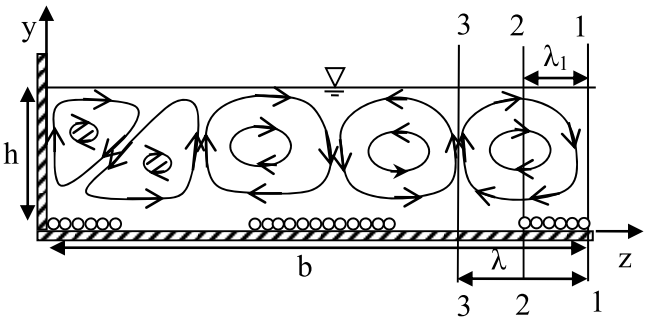

Figure 6. Typical secondary currents induced by sidewall and roughness strips in *Wang and Cheng*'s [2005] experiment. The width of secondary currents is denoted by λ, the width of rough stripe is λ_1. Along profiles 1–1, 2–2 and 3–3, the wall normal velocity is negative (downward), zero and positive (upward), respectively.

both sides of these apexes i.e., "A" and "B," the values of U are different, thus $\partial U/\partial z \neq 0$. According to equation (16), then secondary flow will be generated. As the maximum shear stress occurs at "A" and "B," i.e., the interface between the main channel and floodplain [*Yang et al.*, 2005b], equation (17) dictates that the near-wall secondary flow will move toward these apexes from both sides. This is how the secondary currents are formed in compound channels. Based on the aforementioned discussion, it can be inferred that secondary currents display the following characteristics:

[30] 1) Secondary currents will be generated if there exists a lateral variation of streamwise mean velocity in the near-bed region, or $\partial U/\partial z \neq 0$.

[31] 2) The near-wall secondary flow always moves toward a location where the mean streamwise velocity U or the boundary shear stress τ is higher.

[32] 3) The secondary currents do not intersect division lines, solid boundary or free surface. Thus lines with zero shear stress τ define the domain (size and shape) within which secondary currents are confined and circulated.

5. Quantitative Model for Secondary Currents Induced by Sand Stripes

[33] Lateral variation of roughness results in nonzero $\partial U/\partial z$ and hence secondary currents are observable based on equation (16). This inference is consistent with the experimental observations reported by *McLelland et al.* [1999], *Wang and Cheng* [2005]. The strength of the secondary current is strongest at the interface between roughness change, for example at point 2 of Figure 6. As the near-bed velocity U is non-uniform ($\partial U/\partial z \neq 0$), then the lateral Reynolds shear stress $-\overline{uw}$ must exist (see equation (15)), and there is the corresponding nonzero UW (see equation (14)). As $U \neq 0$, then $W_t \neq 0$, secondary current will be generated.

[34] Equations (9) and (23) state that the standard linear distribution (SLD) of Reynolds shear stress may be observed when and only when the momentum flux $UV_n = 0$. The measured Reynolds shear stress will be higher than that predicted by SLD when $UV_n > 0$, and lower when $UV_n < 0$. In other words, the concave/convex profile of measured Reynolds shear stress reflects the existence of downward/upward secondary currents [see *Yang*, 2007; *Yang and Lee*, 2007].

[35] The Reynolds shear stress is often modeled by

$$-\overline{uv} = u_* \kappa y \left(1 - \frac{y}{h}\right) \frac{\partial U}{\partial y} \tag{24}$$

where κ = Karman constant. It is widely accepted that the parabolic eddy viscosity used in equation (24) is valid for a wide and shallow channel. Inserting equation (24) into equation (23), one has

$$\kappa\xi(1-\xi)\frac{\partial U^+}{\partial \xi} - U^+V^+ = 1 - \xi \tag{25}$$

where $\xi = y/h$, $U^+ = U/u_*$, $V^+ = V/u_*$. Equation (25) describes the influence of secondary current on the velocity distribution. Equation (25) demonstrates that if $V = 0$, the classical log-law can be obtained. If $V < 0$, then $\partial U^+/\partial\xi = 0$ (or maximum velocity) appears below the water surface (dip phenomenon). If $V > 0$, the velocity gradient is higher than the gradient of log-law and wake-function is needed as a correction to the log-law, which is consistent with experimental observations [e.g., *Kironoto and Graf*, 1995].

[36] Integrating equation (25) with respect to ξ, one obtains

$$\frac{U}{u_*} = \frac{1}{\kappa}\exp\left(\int \frac{V^+ d\xi}{\kappa\xi(1-\xi)}\left[\int \frac{1}{\xi}\exp\left(\int \frac{-V^+ d\xi}{\kappa\xi(1-\xi)}\right)d\xi + c\right]\right) \tag{26}$$

where c = integration constant. If $V^+ = 0$, equation (26) reduces into the classical log-law:

$$\frac{u}{u_*} = \frac{1}{\kappa}\ln\frac{\xi}{\xi_0} \tag{27}$$

where $\xi_0 = y_0/h$ and y_0 is the reference level where velocity $U = 0$.

[37] The boundary conditions of wall-normal velocity are: at $\xi = 0$, $V = 0$, and at $\xi = 1$, $V = 0$. One may assume that

$$V^+ = \kappa\alpha\xi^{n_0}(1-\xi)^{n_1}. \tag{28}$$

Approximately, where α, n_0 and n_1 are empirical coefficients to be determined experimentally. Theoretically n_0 and n_1 can be determined using the measured velocity dip that is dependent on the channel geometry, such as the aspect ratio and roughness distributions. As a first approximation, one may assume that $n_0 = n_1 = 1$. Thus equation (26) may be integrated and a simple expression of secondary flow can be obtained. Hence equation (28) becomes

$$\frac{U}{u_*} = \frac{1}{\kappa}e^{\alpha\xi}\left[\int \frac{e^{-\alpha\xi}}{\xi}d\xi + c\right]. \tag{29}$$

By using Taylor series for $e^{-\alpha\xi}$ and boundary conditions as stipulated earlier, and by defining

$$W_1(\alpha,\xi) = \frac{1}{\kappa}\left(e^{\alpha\xi} - 1\right)\ln\frac{\xi}{\xi_o} + \frac{e^{\alpha\xi}}{\kappa}\left[\left(\frac{\alpha\xi}{2}\right)^2 - \alpha\xi\right] \tag{30}$$

one may obtain the velocity distribution as follows:

$$\frac{U}{u_*} = \frac{1}{\kappa}\ln\frac{\xi}{\xi_o} + W_1(\alpha,\xi). \tag{31}$$

The wall-tangent velocity W can be determined by inserting equation (28) into equation (1), and integrating with respect to z yields

$$W^+ = -\kappa(1-2\xi)\frac{\lambda}{h}\int_0^\eta \alpha d\eta \tag{32}$$

where $W^+ = W/u_*$, λ = width of secondary currents cell and $\eta = (b - z)/\lambda$ (see Figure 6). The boundary conditions for W are: at $\eta = 0$, $W = 0$ and at $\eta = 1$, $W = 0$. Then one may simply propose the following equation for W:

$$W^+ = -\kappa(1-2\xi)\frac{\lambda}{h}\alpha_o\eta^m(1-\eta) \tag{33}$$

where α_o = strength of secondary currents, and m is a coefficient. The maximum W should exist where $\partial U/\partial z$ is maximum due to abrupt change of roughness. The coefficient m can be determined by noting that $dW/dz = 0$ at the abrupt change, i.e.,

$$m = \frac{\eta_1}{1-\eta_1} = \frac{\lambda_1}{\lambda-\lambda_1} \tag{34}$$

where $\eta_1 = \lambda_1/\lambda$, λ_1 = half width of the rough strip. If $\lambda_1 = \lambda/2$, then equation (34) gives $m = 1$, which indicates that the maximum wall-tangent velocity W appears at the edge of the rough strip. Comparing equation (32) with (33), one gets

$$\alpha = m\alpha_o\eta^{m-1}\left(1-\frac{m+1}{m}\eta\right). \tag{35}$$

One can determine the unknown variable α_o theoretically if ε_t is known. But unfortunately, as far as the writers are aware of, no reliable ε_t has been published in the literature. Thus α_o should be determined using an alternate approach.

[38] The dip-phenomenon or the maximum velocity occurs below the free surface. Mathematically this implies that $\partial U/\partial\xi = 0$. Thus the relationship between α_o and the dip-phenomenon can be established from equation (25):

$$-U_m^+V_m^+ = 1-\xi_m \tag{36}$$

where the subscript m denotes the location of maximum velocity. The dip-phenomenon or velocity extreme must satisfy the condition of $\partial U/\partial\eta = 0$, or

$$\frac{\partial u}{\partial\eta} = \frac{\partial u}{\partial\alpha}\frac{d\alpha}{d\eta} = 0. \tag{37}$$

Therefore, $d\alpha/d\eta = 0$ at the velocity dip. From equation (35), one can determine the lateral location of velocity-dip as follows

$$\eta_m = \frac{m-1}{m+1}. \tag{38}$$

By inserting equation (34) into equation (38), one has

$$\eta_m = 2\frac{\lambda_1}{\lambda} - 1. \tag{39}$$

Equation (39) indicates that if $\lambda_1/\lambda = 1/2$, the velocity dip occurs at $\eta = 0$, or profile 1–1 in Figure 6. By inserting equation (39) into equation (35), one can determine the coefficient α_m at the wall-normal line of velocity dip as follows:

$$\alpha_m = m\alpha_o\eta_m^{m-1}\left(1-\frac{m+1}{m}\eta_m\right). \tag{40}$$

Further, by inserting equations (28) and (40) into equation (36), the unknown α_o and dip-phenomenon has the following relationship:

$$\alpha_o = -\frac{\eta_m^{1-m}}{\kappa\xi_m U_m^+[m-(m+1)\eta_m]}. \tag{41}$$

Equation (41) provides the means for estimating the strength of secondary currents α_o using the measured maximum streamwise velocity U_m^+ and its location ξ_m and η_m.

6. Data Analysis and Verification

[39] The above discussion explains how the secondary currents are generated and how the strength, size and direction of a cell of secondary currents are determined. *Wang and Cheng*'s [2005] experimental data are used for verification. This set of experiments was conducted in a 0.6 m wide channel where the bed was covered with alternate longitudinal sediment-free and sediment-covered stripes (see Figure 6). The measured parameters include streamwise velocities, secondary currents as well as Reynolds shear stress.

[40] *In Near-Boundary Region. Wang and Cheng* [2005] observed the secondary currents as shown in Figure 6. In their experiment, there existed lateral variations of near-bed velocity, because the sediment strips retarded the flow while the smooth strips corresponded to higher flow speed zones. As expected, secondary currents were generated and the observed secondary currents are shown in Figure 6. Equation (16) also shows that if the lateral gradient of near-bed velocity U is zero, then secondary currents appear. This means that if Wang and Cheng's channel bed was fully covered by homogeneous roughness elements, secondary currents would not have been observable. This inference is consistent with other experiments where the channel bed was uniformly covered by sediment [e.g., *Yassin*, 1953].

[41] Most importantly, equation (16) indicates that the near-boundary secondary flow always moves to a location with higher velocity. Wang and Cheng measured the streamwise mean velocity U along profiles 1–1, 2–2 and 3–3 and the data are reproduced here as Figure 7. Comparing the measured near-bed velocity at profiles 1–1 and 3–3, one can see that $U_3 > U_1$ where U_3 and U_1 are the near-bed velocity at profiles 1–1 and 3–3, respectively (see Figure 7b where the measured data points are linked by solid lines, thus one can see the lateral variation of mean velocity). Based on equation (16), the near-bed secondary flow must have moved from 1 to 1 to 3–3 and drives the clockwise

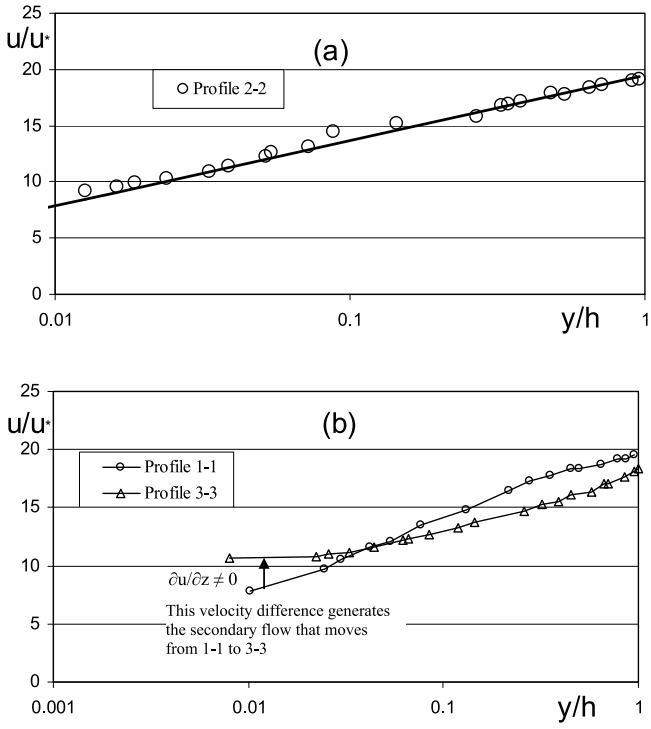

Figure 7. Distributions of the streamwise mean velocity measured by *Wang and Cheng* [2005] along: (a) profile 2–2, where the wall-normal velocity is zero and the measured data can be fitted by a straight line indicating that the streamwise velocity follows the logarithmic distribution; (b) profiles 1–1 and 3–3, showing that the two curves differs from each other.

secondary flow. *Wang and Cheng*'s [2005] measurement confirmed this prediction, see Figure 6.

[42] *In the Main Flow Region.* The above discussion shows that in the main flow region, the wall-normal velocity plays an important role in the mass and momentum transfer. If the wall-normal velocity is zero, equation (23) predicts that the Reynolds shear stress will follow a linear distribution, and equation (26) says that the velocity follows the log-law. From Figure 6, one can see that the wall normal velocity for profile 1–1 is downward ($V < 0$); upward for profile 3–3 ($V > 0$), and parallel to surface for profile 2–2 ($V = 0$). Figure 7a clearly demonstrates that the measured velocity along 2–2 can be represented by a straight line that follows the log-law. Figure 8a also shows that, as expected, the measured Reynolds shear stress can be roughly represented by a straight line, but that along profiles 1–1 and 3–3 is either systematically lower or higher than the linear distribution, as predicted. These deviations are also consistent with equation (23) as the term UV/u_*^2 is negative and positive along the profiles of 1–1 and 3–3, respectively. As predicted by equation (23), the measured Reynolds shear stresses along 1–1 and 3–3 follow the concave and convex distributions as shown in Figure 8a. When the data points in Figure 8a are re-plotted in the form of $(-\overline{uv} - UV)/u_*^2$ against y/h, all the data points cluster along the line as shown in Figure 8b, suggesting that the difference between the measured Reynolds shear stress and the straight line in Figure 8a is in fact attributable to the term UV/u_*^2. The noticeable discrepancy could be caused by two sources: 1) the data U and V at every point were estimated from published graphs, which could have introduced some errors, especially for the data V; 2) *Wang and Cheng* [2005] did not perform 3-D velocity measurement directly. Instead they measured 2 components of secondary flow, and the third component was obtained using the continuity equation, which could introduce some errors also.

[43] *Strength of Secondary Currents.* The wall-normal and wall-tangent velocities V and W can be calculated using equations (28) and (33). Figure 9 shows the comparison of measured and predicted velocity components of secondary currents. The agreement is acceptable, indicating that the secondary currents originate from the boundary and the lateral gradient of near-bed velocity is the driving force. This fact can be discerned from Figure 9 in which the highest near-bed velocity, W, occurs at the location where there exists a sharp variation of stripe roughness, i.e., at 2–2, whereas at the bottom of 1–1 and 3–3, $\partial U/\partial z \approx 0$ as there is no roughness variation in its vicinity. Consequently the value of W is ≈ 0. We may deduce that larger $\partial U/\partial z$ corresponds to larger W, and smaller $\partial U/\partial z$ corresponds to smaller W, i.e., W should be proportional to $\partial U/\partial z$.

[44] The dip-phenomenon always associates with the downward velocity V. Thus the wall-normal line through the point of velocity dip is a division line. A second wall-

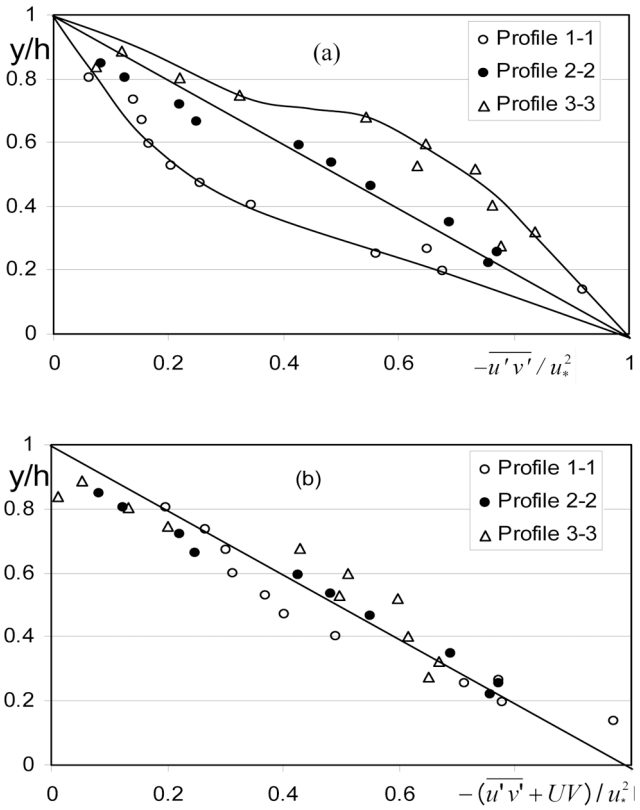

Figure 8. Distribution of measured Reynolds shear stress by *Wang and Cheng* [2005] along different profiles (1–1, 2–2 and 3–3) when plotted in the form of: (a) $-\overline{u'v'}/u_*^2$; and (b) $\left(-\overline{u'v'} - UV\right)/u_*^2$.

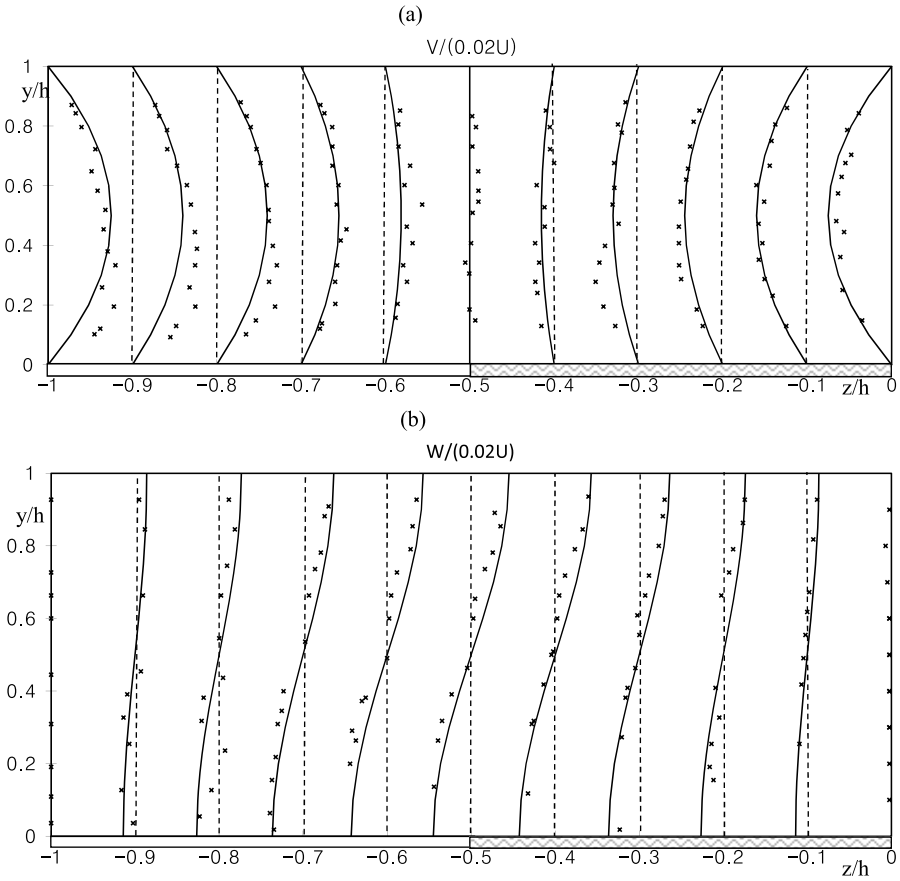

Figure 9. Distributions of the measured secondary velocities by *Wang and Cheng* [2005]: (a) vertical mean velocity V; and (b) spanwise mean velocity W. The cross symbol represents the measured velocity that is scaled to the distance between two neighboring dashed lines, which is take to be unity. The solid lines are calculated from equations (28) and (33). The dashed vertical lines are the profiles for the velocity measurement. The bars without shadows denote the smooth boundaries, while the roughened strips are represented by bars with shadows.

normal line through the mid-point between two neighboring velocity-dip points establishes the second division line. Therefore, based on the locations of maximum velocity and equation (41), one obtains that $\alpha_0 = 0.42$, and from equation (35), $\alpha = 0.21$. The strength of secondary currents can be determined using equation (36) based on the information of velocity-dip.

7. Sediment Transport, Secondary Currents and Morpho-dynamics

[45] The sediment patterns of stripes and ridges are attributable to secondary currents [*Vanoni*, 1946; *Nezu and Nakagawa*, 1993]. The following discussion may provide evidence that secondary currents are both the cause as well as the results of the sediment patterns and the geomorphologic patterns observed. For a channel flow, the governing equation of sediment transport can be written as follows:

$$\frac{\partial C}{\partial t}+\frac{\partial\left(UC+\overline{u'C'}\right)}{\partial x}+\frac{\partial\left(VC+\overline{v'C'}\right)}{\partial y}+\frac{\partial\left(WC+\overline{w'C'}\right)}{\partial z}=\frac{\partial(C\omega)}{\partial y} \tag{42}$$

where C is the sediment concentration and ω the falling velocity of particles. For a steady and uniform flow, and consider the vertical direction only, equation (42) may be simplified as

$$\overline{v'C'}=\varepsilon_s\frac{dC}{dy}=C(\omega-V) \tag{43}$$

where ε_s is the diffusion coefficient. Obviously if $V = 0$ (e.g., profile 2–2 in Figure 6), the Rouse equation can be derived from equation (43). If $V > 0$ or the direction of the secondary flow is upward, the net settling velocity is smaller (e.g., profile 3–3 in Figure 6), the gradient of sediment concentration, dC/dy will become smaller. If $\omega = V$, the concentration gradient dC/d$y = 0$, or surface sediment concentration will be the same as that at the bed since the gradient is zero. This is why Nezu and Nakagawa (see Table 1) observed high sediment concentration in the upflow zone and divergent boil lines on its surface. On the other hand, if the secondary flow is downward (e.g., profile 1–1 in Figure 6), the net settling velocity will be higher than ω, and the increased falling velocity of particle will increase the value of dC/dy. Consequently, the sediment concentration near the free

surface is relatively low. The downward secondary currents form a convergent downward flow, driving the sediment downward, as observed by Nezu and Nakagawa. This deduction explains why one can detect the upward/downward flows based on aerial photographs [*Kinoshita*, 1967] or satellite images over river/ocean surface. Therefore, it can be seen that there exists a lateral variation of sediment concentration. The cumulative effect of this lateral variation results in the formation of sediment patterns on the bed. Thus one can conclude that secondary currents play a dominant role in sand ridges and stripes' formation.

[46] It should be mentioned that this study discusses only the formation of secondary current caused by sand ridge and sediment stripes and its influence on sediment transport in open channel flows as shown in equation (43). Nevertheless the results can be easily extended to explain the widely observed sand ridges on the continental shelf [*Trowbridge*, 1995; *Garnier et al.*, 2010] or wind-blown sand ridges in the deserts [*Liao et al.*, 2010]. In fact, the discussion can also be extended to explain the sand ridges formed near wrecks which were observed and reported by *Karcz* [1981], *Schlichting* [1979] and *McLean* [1981]. In other words, a small isolated obstacle on a river bed, such as a rock, a wreck or a boulder, can trigger secondary currents that in turn create a sand ribbon in its vicinity.

8. Discussion

[47] It can be seen from the above discussion, in the absence of corner-related secondary flows, spanwise variations in bed topography or boundary roughness can also lead to the formation of secondary flows. The latter has been termed as stress-induced. However, equation (16) reveals that the secondary flows are more likely to be boundary-induced. *Nezu and Nakagawa* [1984] and *Wang and Cheng* [2005] demonstrated that flow over fixed-ridges produces stable secondary flows with upflow over the ridge crests and downflow into the adjacent troughs. Similarly, for an erodible bed with homogeneous sediments, regular ridges and troughs are observed in the central region of the channel. These secondary currents, independent of the secondary flow at the corners, are triggered by the lateral variation of near-boundary velocity. This observation suggests that the principle mechanism underlying the formation of sediment ridges is instability dynamic process that is initiated by a non-uniform cross-stream distribution of streamwise velocity. Consequently, secondary flow can be amplified by the deformation of mobile bed sediments until an equilibrium condition between the lateral sediment transport and secondary flow is established. In poorly sorted sediments, the secondary currents can generate a pattern of alternate coarse- and fine-grain sediment stripes. These phenomena can be explained using the lateral variation of boundary shear stress. Once the boundary shear stress is non-uniformly distributed in the transverse direction, secondary flows would be generated. One can see that it does not matter which one of the two processes, secondary currents or non-uniform bed roughness, comes first. As long as a small perturbation takes place, the two processes reinforce each other until a dynamic equilibrium state is reached. The near-boundary secondary flow can transport sediment, which in turn further results in the propagation of secondary currents. Therefore, sand ridges and troughs are observed in a very wide channel bed. This inference is consistent with *McLelland et al.* [1999], who observed that boundary shear stress is maximized over the coarse-grained stripe, and minimized over the fine-grained bed stripe, i.e., areas of high boundary shear stress relate to the coarse-grained stripe and conversely for the fine-grained stripe. This is because the coarse-grained strip is always associated with downward secondary flow that carries high momentum that entrained the smaller sediment particles, leaving coarser particles behind. Conversely the upward flow always appears in the zone within the fine-grained stripes, where the fine particles originates from elsewhere.

[48] Similarly, lateral variation of boundary shear stress can also explain the formation of sand ridges on an infinitely wide bed. Troughs can be formed when the boundary shear stress exceeds the critical shear stress and sediment settles where the boundary shear stress is less than the critical threshold for initial motion. Thus, spatial variations in local bed load transport are the result of non-uniform distribution of boundary shear stress and the secondary currents that are generated. A similar correlation between the magnitude of the boundary shear stress and bed load transport has also been described by *Hirano and Ohmoto* [1988] and *Nezu and Nakagawa* [1989] for self-formed sand ridges in unimodal sediments.

[49] There are a number of competing hypotheses to explain the formation of sand ridges in the literature, which have been advanced to account for the presence of ridge–runnel systems [*Carling et al.*, 2009], but none of them can explain all the observed phenomena. Among them, the vorticity model of *Colombini* [1993] does not account for the influence of evolving bathymetry, while the importance of evolving bathymetry for the formation of secondary currents has been stressed by *Whitehouse et al.* [2000] and *Franca and Lemmin* [2006]. These authors have the view which is consistent with the present study's result. Our studies suggest that the multicellular secondary currents exhibit some form of self-organization triggered by the wall or the anisotropic properties of bed roughness. For a loose boundary, these secondary currents could be enhanced and propagated laterally due to the lateral sediment transport, i.e., the presence of ridge-runnel systems.

9. Conclusions

[50] The mechanism for initiation and sustained development of secondary currents (Prandtl's second kind) has been investigated. By examining the Reynolds equation in the boundary region, we reveal that the secondary currents originate from the boundary region. In other words, the lateral variation of streamwise velocity ($\partial U/\partial z \neq 0$) yields the secondary currents. The main findings of the present study can be summarized as follows:

[51] 1. The tangential velocity W in the near-bed region exists to balance the transverse Reynolds shear stress $-\rho\overline{uw}$ that is always associated with the lateral variation of streamwise mean velocity. Consequently the secondary flow drives a circulation in certain prescribed domain, and turbulence anisotropy appears in the main flow region. Thus the driving force to initiate the secondary currents of the

Prandtl's second kind is the transverse Reynolds shear stress $-\rho\overline{uw}$ or $\partial U/\partial z$.

[52] 2. The source of secondary currents is the near-bed region, rather than the main flow region. In other words, any small disturbance on the bed flow region may trigger secondary currents, which subsequently result in the anisotropy of turbulence in the main flow region. The interactions between the turbulence anisotropy and the secondary flow can be inferred from equation (23) and from experimental results listed in Table 1. Hence, the boundary is not only the primary source of turbulence, but also the source of secondary currents. In other words, without external forces all sustainable eddies come from boundary with velocity variation, $\partial U/\partial x \neq 0$ yields large scale eddies; $\partial U/\partial y \neq 0$ yields small size eddies or turbulence, and $\partial U/\partial z \neq 0$ yields the secondary currents.

[53] 3. The near-bed secondary flow is always from lower to higher velocity zone. The largest secondary flow is observed at the location where the near-bed velocity U changes abruptly (e.g., from floodplain to main channel). Secondary currents are not observable where the near-bed velocity U remains unchanged laterally.

[54] 4. The relationship between the boundary shear stress and secondary currents has been established. The findings show that the near-wall secondary flow always moves from the location with lower boundary shear stress to that with higher boundary shear stress. Higher boundary shear stress is always associated with downward flow, and lower boundary shear stress appears at the region with upward flow.

[55] 5. A theoretical framework has been established to describe the influence of secondary currents on sediment transport. It has been shown that the upward flow always promotes sediment transport, but the downward flow constrains the entrainment of sediment. In other words, with the presence of time-averaged wall-normal velocity, the same sediment particles have relatively higher mobility in the zone with upward flow, but their mobility is reduced in the zone of downward flow. This lateral imbalance of mobility leads to the formation of sand ridges.

Notation

A area [L^2]
b width of channel [L]
c integration constant
g gravitational acceleration [L/T^2]
h water depth [L]
k slope of division line
m coefficient
n_o coefficient
n_1 coefficient
p wetted perimeter [L].
S energy slope
u_* shear velocity [L/T]
U, V, W mean velocity in x, y, z directions, respectively [L/T]
u, v and w turbulent velocity fluctuations [L/T]
$-\overline{uv}/u_*^2$, $-\overline{uw}/u_*^2$ dimensionless Reynolds shear stress
U^+ U/u_*
V^+ V/u_*
V_n velocity in direction Normal to the boundary [L/T]
W^+ W/u_*
W_1 wake function
y_0 reference level [L]
x streamwise direction
y wall-normal direction
z wall-tangent direction
α coefficient
α_o coefficient.
ε_t turbulent eddy viscosity
Ω vorticity [1/L]
η $(b/2 - z)/\lambda$
κ Karman constant
λ width of secondary currents [L]
ξ y/h
ξ_0 y_0/h
ρ fluid density [ML^{-3}]
τ total shear stress [N/L^2]
$\bar{\tau}_w$ mean sidewall shear stress [N/L^2]
μ dynamic viscosity [NT/L^2]
ν kinematic viscosity of fluid [L^2/T].

[56] **Acknowledgments.** The research presented in this paper has been supported in part, by the open fund (SKLH-OF-1002) provided by State Key Laboratory of Hydraulics and Mountain River Engineering at Sichuan University, and the National Natural Science Foundation of China (51239001) and (51228901).

References

Albayrak, I. (2008), An experiment study of coherent structures, secondary currents and surface boils and their interrelation in open-channel flow, PhD thesis, École Polytechnique Fédérale de Lausanne, Lausanne, Switzerland.

Blanckaert, K., and W. H. Graf (2004), Momentum transport in sharp open-channel bends, *J. Hydrol. Eng.*, *130*(3), 186–198, doi:10.1061/(ASCE)0733-9429(2004)130:3(186).

Boussinesq, J. (1877), *Essai sur la théorie des eaux courantes*, Impimerie Nationale, Paris.

Bradshaw, P. (1987), Turbulent secondary flows, *Annu. Rev. Fluid Mech.*, *19*, 53–74, doi:10.1146/annurev.fl.19.010187.000413.

Brundrett, E., and W. D. Baines (1964), The production and diffusion of vorticity in duct flow, *J. Fluid Mech.*, *19*, 375–394, doi:10.1017/S0022112064000799.

Carling, P. A., J. J. Williams, I. W. Croudace, and C. L. Amos (2009), Formation of mud ridge and runnels in the intertidal zone of the Severn Estuary, UK, *Cont. Shelf Res.*, *29*, 1913–1926, doi:10.1016/j.csr.2008.12.009.

Colombini, M. (1993), Turbulence driven secondary flows and the formation of sand ridges, *J. Fluid Mech.*, *254*, 701–719, doi:10.1017/S0022112093002319.

Cooper, J. R., and S. J. Tait (2008), The spatial organization of time-averaged streamwise velocity and its correlation with the surface topography of water-worked gravel bed, *Acta Geophys.*, *56*(3), 614–641, doi:10.2478/s11600-008-0023-0.

Culbertson, L. K. (1967), Evidence of secondary circulation in an alluvial channel, *U.S. Geol. Surv. Prof. Pap.*, *575-D*, 214–216.

Einstein, H. A., and H. Li (1956), The viscous sublayer along a smooth boundary, *J. Eng. Mech. Div.*, *82*, 1–27.

Flintham, T. P., and P. A. Carling (1988), The prediction of mean bed and wall boundary shear in uniform and compositely rough channels, in *River Regime*, edited by R. White, pp. 267–287, John Wiley, Chichester, U. K.

Flintham, T. P., and P. A. Carling (1989), Manning's-N of composite roughness in channels of simple cross section, in *Proceedings of the International Conference for Centennial of Manning's Formula and Kuichling's Rational Formula*, edited by B. C. Yen, pp. 518–529, Am. Soc. Civ. Eng., Reston, Va.

Franca, M. J., and U. Lemmin (2006), Cross-section periodicity of turbulent gravel-bed river flows, in *River, Coastal and Estuarine Morphodynamics*, edited by G. Parker and M. H. Garcıía, pp. 203–210, Taylor and Francis, New York.

Galletti, B., and A. Bottaro (2004), Large-scale secondary structures in duct flow, *J. Fluid Mech.*, *512*, 85–94, doi:10.1017/S0022112004009966.

Garnier, R., N. Dodd, A. Falques, and D. Calvete (2010), Mechanisms controlling crescentic bar amplitude, *J. Geophys. Res.*, *115*, F02007, doi:10.1029/2009JF001407.

Gavrilakis, S. (1992), Numerical simulation of low Reynolds-number turbulent flow through a straight square duct, *J. Fluid Mech.*, *244*, 101–129, doi:10.1017/S0022112092002982.

Gerard, R. (1978), Secondary flow in noncircular conduits, *J. Hydraul. Div. Am. Soc. Civ. Eng.*, *104*, 755–773.

Gessner, F. B. (1973), The origin of secondary flow in turbulent flow along a corner, *J. Fluid Mech.*, *58*, 1–25, doi:10.1017/S0022112073002090.

Hirano, M., and T. Ohmoto (1988), Experimental study on the interaction of between longitudinal vortices and sand ribbons, in *Proceedings of the 6th Congress*, vol. 2, pp. 59–65, APD-IAHR, Madrid.

Karcz, I. (1981), Reflections on the origin of small scale longitudinal streambed scours, in *Fluvial Geomorphology: A Proceedings of the Forth Annual Geomorphology Symposia Series*, edited by M. Morisawa, pp. 149–177, Allen and Unwin, London.

Karl, H. A. (1980), Speculations on processes responsible for mesoscale current lineations on the continental shelf, southern California, *Mar. Geol.*, *34*, M9–M18.

Kenyon, N. H. (1970), Sand ribbons of European tidal seas, *Mar. Geol.*, *9*, 25–39.

Kinoshita, R. (1967), An analysis of the movement of flood waters by aerial photography, concerning characteristics of turbulence and surface flow, *Photogr. Surv.*, *6*, 1–17.

Kironoto, B. A., and W. H. Graf (1995), Turbulence characteristics in rough non-uniform open-channel flow, *Proc. ICE Water Mar. Energy*, *112*, 336–348.

Knight, D. W., and H. S. Patel (1985), Boundary shear in smooth rectangular ducts, *J. Hydrol. Eng.*, *111*(1), 29–47, doi:10.1061/(ASCE)0733-9429(1985)111:1(29).

Liao, K., J. Qu, J. Tang, F. Ding, H. Liu, and S. Zhu (2010), Activity of wind-blown sand and the formation of feathered sand Ridges in the Kumtagh Desert, China, *Boundary Layer Meteorol.*, *135*, 333–350, doi:10.1007/s10546-010-9469-0.

Lim, S. Y., and S. Q. Yang (2005), Simplified model of tractive-force distribution in closed conduits, *J. Hydraul. Eng.*, *131*(4), 322–329, doi:10.1061/(ASCE)0733-9429(2005)131:4(322).

McLean, S. R. (1981), The role of non-uniform roughness of sand ribbons, *Mar. Geol.*, *42*, 49–74, doi:10.1016/0025-3227(81)90158-4.

McLelland, S. J., P. J. Ashworth, J. L. Best, J. Roden, and G. J. Klaassen (1999), Flow structure and spatial distribution of suspended sediment around an evolving braid bar, Jamuna River, Bangladesh, in *Fluvial Sedimentology VI*, *Int. Assoc. Sedimentol. Spec. Publ.*, vol. 28, edited by N. D. Smith and J. Rogers, pp. 43–57, Gent, Belgium.

Nezu, I., and H. Nakagawa (1984), Cellular secondary currents in a straight conduit, *J. Hydr. Eng.*, *110*, 173–193.

Nezu, I., and H. Nakagawa (1989), Self-forming mechanism of longitudinal sand ridges and troughs in fluvial open channel flows, in *Proceedings of the 23rd Congress*, pp. B65–B72, IAHR, Madrid.

Nezu, I., and H. Nakagawa (1993), *Turbulence in Open-Channel Flows*, A. A. Balkema, Rotterdam, Netherlands.

Nezu, I., and W. Rodi (1985), Experimental study on secondary currents in open channel flows, in *Proceedings of the 21st Congress*, vol. 2, pp. 115–119, IAHR, Madrid.

Nezu, I., H. Nakagawa, and N. Kawashima (1988), Cellular secondary currents and sand ribbons in fluvial channel flows, in *Proceedings of the 6th Congress*, vol. 2, pp. 51–58, APD-IAHR, Madrid.

Nikora, V., and A. G. Roy (2010), Secondary flows in rivers: Theoretical framework, recent advances, and current challenges, paper presented at Conference on Gravel-Bed River 7, Int. Assoc. for Hydraul. Res., Tadoussac, Canada.

Perkins, H. J. (1970), The formation of streamwise vorticity in turbulent flow, *J. Fluid Mech.*, *44*, 721–740, doi:10.1017/S0022112070002112.

Prandtl, L. (1905), *Verhandlungen des dritten internationalen Mathematiker-Kongresses in Heidelberg 1904*, edited by A. Krazer, Teubner, p. 484, Leipzig, Germany. [English translation in *Early Developments of Modern Aerodynamics*, edited by J. A. K. Ackroyd, B. P. Axcell, and A. L. Ruban, Butterworth- Heinemann, Oxford, UK, 2001.]

Prandtl, L. (1952), Uber die ausgebildete Turbulenz, *ZAMM*, *5*, 136–139.

Rhodes, D. G., and D. W. Knight (1994), Distribution of shear force on boundary of smooth rectangular duct, *J. Hydrol. Eng.*, *120*(7), 787–807, doi:10.1061/(ASCE)0733-9429(1994)120:7(787).

Rodriguez, J. F., and M. H. Garcia (2008), Laboratory measurements of 3-D flow patterns and turbulence in straight oen channel with rough bed, *J. Hydraul. Res.*, *46*, 454–465, doi:10.3826/jhr.2008.2994.

Sambrook Smith, G. H., and R. I. Ferguson (1996), The gravel-sand transition: Flume study of channel response to reduce slope, *Geomorphology*, *16*, 147–159, doi:10.1016/0169-555X(95)00140-Z.

Schlichting, H. (1979), *Boundary-Layer Theory*, 7th ed., McGraw Hill, New York.

Shiono, K., and D. W. Knight (1991), Turbulent open-channel flows with variable depth across the channel, *J. Fluid Mech.*, *222*, 617–646, doi:10.1017/S0022112091001246.

Tamburrino, A., and J. S. Gulliver (1999), Large flow structures in a turbulent open channel flow, *J. Hydraul. Res.*, *37*(3), 363–380, doi:10.1080/00221686.1999.9628253.

Tracy, H. J. (1965), Turbulent flow in a three-dimensional channel, *J. Hydr. Eng.*, *91*(6), 9–35.

Trowbridge, J. H. (1995), A mechanism for the formation and maintenance of shore-oblique sand ridges on storm-dominated shelves, *J. Geophys. Res.*, *100*(C8), 16,071–16,086, doi:10.1029/95JC01589.

Tsujimoto, T. (1989), Longitudinal strips of alternate sorting due to cellular secondary currents, in *Proceedings of the 23rd Congress*, B17–B25, IAHR, Madrid.

Vanoni, V. A. (1946), Transportation of suspended sediment by water, *Trans. Am. Soc. Civ. Eng.*, *111*, 67–133.

Wang, Z. Q., and N. S. Cheng (2005), Secondary flows over artificial bed strips, *Adv. Water Resour.*, *28*(5), 441–450, doi:10.1016/j.advwatres.2004.12.008.

Webel, G., and Schatzmann, M. (1984), Transverse mixing in open channel flow, *J. Hydr. Eng.*, *110*(4), 423–435.

Whitehouse, R. J. S., P. Bassoullet, K. R. Dyer, H. J. Mitchener, and W. Roberts (2000), The influence of bedforms on flow and sediment transport over intertidal mudflats, *Cont. Shelf Res.*, *20*, 1099–1124, doi:10.1016/S0278-4343(00)00014-5.

Williams, J. J., P. A. Carling, C. L. Amos, and C. Thompson (2008), Field investigation of ridge–runnel dynamics on an intertidal mudflat, *Estuarine Coastal Shelf Sci.*, *79*, 213–229, doi:10.1016/j.ecss.2008.04.001.

Yang, S. Q. (2007), Turbulent transfer mechanism in sediment-laden flow, *J. Geophys. Res.*, *112*, F01005, doi:10.1029/2005JF000452.

Yang, S. Q., and J. W. Lee (2007), Reynolds shear stress distributions in a gradually varied flow, *J. Hydraul. Res.*, *45*(4), 462–471, doi:10.1080/00221686.2007.9521780.

Yang, S. Q., and S. Y. Lim (1997), Mechanism of energy transportation and turbulent flow in a 3D channel, *J. Hydr. Eng.*, *123*(8), 684–692.

Yang, S. Q., and S. Y. Lim (1998), Boundary shear stress distribution in smooth rectangular open channel flows, *Proc. Int. Civ. Eng. Water Mar. Energy*, *130*(9), 163–173.

Yang, S. Q., and S. Y. Lim (2005), Boundary shear stress distribution in trapezoidal channels, *J. Hydraul. Res.*, *43*(1), 98–102, doi:10.1080/00221680509500114.

Yang, S. Q., and S. Y. Lim (2006), Shear stress in smooth rectangular open-channel flows: Discussion, *J. Hydr. Eng.*, *132*(6), 629–631.

Yang, S. Q., and A. J. McCorquadale (2004), Determination of boundary shear stress and Reynolds shear stress in smooth rectangular channel flows, *J. Hydraul. Eng.*, *130*(5), 458–462, doi:10.1061/(ASCE)0733-9429(2004)130:5(458).

Yang, S. Q., S. Y. Lim, and A. J. McCorquadale (2005a), Investigation of near wall velocity in 3-D smooth channel flows, *J. Hydrol. Res.*, *43*(2), 149–157, doi:10.1080/00221686.2005.9641231.

Yang, S. Q., S. K. Tan, and S. Y. Lim (2005b), Flow resistance and bed form geometry in a wide alluvial channel, *Water Resour. Res.*, *41*, W09419, doi:10.1029/2005WR004211.

Yassin, A. (1953), *Mean Roughness Coefficient in Open Channels With Different Roughness of Bed and Sidewalls*, Verlag Leemann, Zurich.